Applied Catalysis B: Environmental 97 (2010) 151–159

Contents lists available at ScienceDirect

Applied Catalysis B: Environmental

journal homepage: www.elsevier.com/locate/apcatb

The remarkable effect of vanadium doping on the adsorption and catalytic activity of magnetite in the decolorization of methylene blue

Xiaoliang Liang[a,b], Sanyuan Zhu[a], Yuanhong Zhong[a,b], Jianxi Zhu[a], Peng Yuan[a], Hongping He[a,*], Jing Zhang[c]

[a] Guangzhou Institute of Geochemistry, Chinese Academy of Sciences, Guangzhou 510640, China
[b] Graduate University of the Chinese Academy of Sciences, Beijing 100049, China
[c] Institute of High Energy Physics, Chinese Academy of Sciences, Beijing 100049, China

ARTICLE INFO

Article history:
Received 7 February 2010
Received in revised form 17 March 2010
Accepted 26 March 2010
Available online 2 Aprril 2010

Keywords:
Vanadium doped magnetite
Synthesization
Characterization
Adsorption
Degradation

ABSTRACT

In this study, a series of vanadium doped magnetites ($Fe_{3-x}V_xO_4$, $0 \le x \le 0.34$) was synthesized by a precipitation–oxidation route and show good adsorption and catalytic activities. Powder X-ray diffraction (PXRD) and Mössbauer spectra analysis of $Fe_{3-x}V_xO_4$ confirm the formation of magnetite, while Fourier transform infrared spectroscopy (FTIR), Mössbauer spectroscopy and X-ray absorption fine structure (XAFS) spectra indicate vanadium preferentially occupies the octahedral site. The valency of vanadium in magnetite is mainly +3, as inferred from FTIR and XAFS. Thermal analysis (TG–DSC) shows that the incorporation of vanadium in magnetite structure leads to an increase of superficial hydroxyl groups and a decrease in temperature of phase transformation maghemite–hematite. Vanadium incorporation can promote the adsorption of methylene blue (MB) on $Fe_{3-x}V_xO_4$ and degradation of the dye with high degree of decolorization. The improvement of adsorption activity may be related to the increase of superficial hydroxyl. The high catalytic activity is related to the improvement of adsorption activity, the intensification of H_2O_2 decomposition by vanadium on the magnetite surface to produce •OH and the improvement of electron transfer by vanadium to produce a more efficient regeneration of the Fenton active specie Fe^{2+}.

1. Introduction

The application of mineral materials in environment is currently generating much interest due to its strong purification functions, optimal environmental harmony and low operation cost [1–3]. Most of mineral materials can be extensively used in pollution treatment and environmental remediation with the mechanism of surface adsorption, porous filtration, defect of crystal structure, ionic exchange, redox, mineralogical–biological interaction and so on. For example, natural rutile TiO_2 shows powerful photocatalytic activity in degradation of organic pollutants [4]. Montmorillonite, zeolite and their modified products are effective adsorbents to remove aromatic contaminants [5–8]. Natural iron sulfides can treat Cr(VI)-bearing wastewater, reducing Cr(VI) and simultaneously precipitating Cr(III) [9]. The natural self-purification function of minerals improves its application in pollution treatment and controls the geochemical processes of contaminants.

Magnetite (Fe_3O_4) has been vigorously pursued as environmentally friendly and inexpensive catalyst in heterogeneous Fenton system [10]. Ferrous and ferric ions in the structure can activate H_2O_2 and generate hydroxyl radicals (•OH) according to the classic Haber–Weiss mechanism. •OH can unselectively attack and decompose organic contaminants. This process is heterogeneous and can be operated at basic and near neutral pH, which is of considerable interest since it could offer some advantages, such as easy operation, no sludge generation and the possibility of recycling the promoter [11].

Magnetite has a cubic spinel structure with one quarter of the tetrahedral (T_d) and one half of the octahedral (O_h) sites filled by Fe cations. The formula for magnetite is $(Fe^{3+})[Fe^{2+}Fe^{3+}]O_4$ where Fe^{3+} is equally split between (T_d) and [O_h] sites. Fe^{2+} occupies only O_h sites resulting in a distribution for stoichiometic magnetite of 1:1:1 at the Fe d^6O_h:d^5T_d:d^5O_h. Magnetite is extensively distributed on the earth surface [12]. Chemical analysis of natural magnetites suggests that a pure magnetite is rare in nature and isomorphous substitution widely exists in natural magnetites, i.e., ferric and ferrous ions can be replaced by divalent Co, Ni, Zn and Mn, trivalent V and Cr and tetravalent Ti [13]. Crystal-field stabilization, oxidation state and ionic radius effect result in the general preference of Ni^{2+}, Co^{2+}, Mn^{2+} and Fe^{2+} for the O_h site, whereas Zn^{2+} has a very strong

* Corresponding author. Present address: Guangzhou Institute of Geochemistry, Chinese Academy of Sciences, 511 Kehua Street, Guangzhou 510640, Guangdong, China. Tel.: +86 20 85290257; fax: +86 20 85290708.
E-mail address: hehp@gig.ac.cn (H. He).

0926-3373/$ – see front matter.
doi:10.1016/j.apcatb.2010.03.035

affinity for the T_d site [12]. These substitutions significantly influence the physical–chemical properties of nano-particles, making them suitable for customizing a range of different technological applications. These influences depend on the substitution site, nature and the amount of doping cations incorporated into the spinel structure [14,15]. A good understanding of the substitution and site occupancies is a vital step in developing these nanoparticles. Recent studies reveal that the incorporation of metal in the spinel structure brings great effect to the physical–chemical properties of magnetite. For example, Cr has a stabilization effect on the maghemite structure while Mn significantly decreases the temperature of phase transformation maghemite–hematite [16]. Moreover, the introduction of Co, Mn and Cr remarkably improve catalytic activity of the resulting magnetite in heterogeneous Fenton reaction while Ni inhibits the reaction [11].

Vanadium doped magnetite is a very common type of natural magnetite and an important host of iron and vanadium. Naturally occurring vanadium doped magnetite is frequently intergrown with titanomagnetite, forming a very famous natural magnetite in China, vanadium–titanium magnetite [17,18]. Titanomagnetite has been investigated by a previous study in term of metal valency, cations occupancy, thermal stability, adsorption property and catalytic activity [19]. However, the relative studies about vanadium doped magnetite have rarely been involved and the effect of vanadium on the physical–chemical properties of magnetite has not been sufficiently confirmed, which may greatly hinder the industrial applications of this mineral material. As the valency of vanadium in natural magnetite structure is mainly +3, the redox property of vanadium in the structure may be an important factor of physical–chemical properties of the doping magnetite.

Hence, in this study, a series of vanadium doped magnetites ($Fe_{3-x}V_xO_4$) with different vanadium content has been prepared using a precipitation–oxidation method. The synthetic $Fe_{3-x}V_xO_4$ was characterized by a variety of techniques. Four aspects are concentrated on in this study: (i) the valency and occupied site of vanadium in spinel structure; (ii) effect of vanadium on the physical–chemical properties of $Fe_{3-x}V_xO_4$; (iii) the adsorption capacity of $Fe_{3-x}V_xO_4$ for organic contaminants; (iv) the catalytic performance of $Fe_{3-x}V_xO_4$. In addition, methylene blue (MB) was selected as a model contaminant since it is non-biodegradable and extensively used in textile industry. This study is of high importance to well understand the influence of vanadium doping on the physical–chemical properties of magnetite. Also, this is a crucial point to explore the interaction mechanism between natural vanadium–titanium magnetite and organic contaminants, which is benefit for the application of this mineral in environmental decontamination and knowledge of the transfer and transformation of organic contaminants on the earth surface.

2. Experimental

2.1. Preparation of $Fe_{3-x}V_xO_4$

All chemicals and reagents used in this work were of analytical grade and used as received.

Predetermined amount of ferrous sulfate was dissolved in HCl solution. 1.0 mL hydrazine was added to prevent the oxidation of ferrous cations, and pH was low enough (<1) to prevent iron oxidation and hydroxide precipitation. This solution was heated to 90–100 °C. Equal volumes of a solution containing 4.0 mol L^{-1} NaOH, 0.90 mol L^{-1} $NaNO_3$ and suitable amount of ammonium metavanadate was added dropwise (10 mL min^{-1}) into the heated iron solution and the reaction was maintained at 90 °C for 2 h, while stirring at a rate of 500 rpm. Then the solution was cooled to room temperature. It was necessary to emphasize that during the reaction, N_2 was passed through to prevent the oxidation of ferrous cation by air. In the final solution, the total metal cation concentration of Fe and V was 0.45 mol L^{-1}. The particles were then separated by centrifugation at 3500 rpm for 5 min and washed with boiling distilled water, followed by an additional centrifugation. After 3–4 washings, the particles were collected and dried in a vacuum oven at 100 °C for 24 h [19,20].

Also, Fe_3O_4 was synthesized using above procedure without adding ammonium metavanadate. All the samples were ground and passed through a 200 mesh screen.

2.2. Characterization methods

Total Fe content was measured spectrophotometrically with the phenanthroline method and Fe^{2+} content was analyzed by K_2CrO_4 titration. Fe^{3+} content was obtained by subtracting Fe^{2+} content from total Fe content. Vanadium content was determined spectrophotometrically with the tungstovanadophosphoric acid method [21].

Powder X-ray diffraction patterns (PXRD) were recorded between 10° and 80° (2θ) at a step of 1° min^{-1} using a Bruker D8 advance diffractometer with Cu Kα radiation (40 kV and 40 mA).

Fourier transform infrared spectra (FTIR) were recorded on Bruker Vector 70 Fourier transform infrared spectrometer. Specimens for measurement were prepared by mixing 0.9 mg of the sample powder with 70 mg of KBr. Then each mixture was pressed into a pellet. Sixty-four scans were collected for each measurement in the spectral range of 370–1000 cm^{-1} with a resolution of 4 cm^{-1}.

For ^{57}Fe Mössbauer measurement, 250–335 mg of the powder sample without any chemical pretreatment was gently pressed into a brass sample holder (16 mm in diameter, 1 mm thick). The sample holder was closed on two ends with iron free plastic tap. The Mössbauer spectra were obtained with a Mössbauer spectrometer Austin Science S-600 using a γ-ray source of 1.11 GBq ^{57}Co/Rh at a consistent temperature (293 K). Spectra were fitted to Lorentzian lineshapes using standard line shape fitting routines with a personal computer. Half-width (HW) and peak intensity of each quadruple doublet was constrained to be equal. Isomer shifts (IS) were expressed with respect to the centered of the spectrum of metallic iron foil.

The V K-edge X-ray absorption fine structure (XAFS) spectra of $Fe_{3-x}V_xO_4$ samples and reference compounds were collected on beamline 1W1B of Beijing Synchrotron Radiation Facility (BSRF). The BSRF storage ring is operated at the electron energy of 2.2 GeV with beam current of 250 mA. The 1W1B is a focused X-ray beamline, using a Si (1 1 1) double crystal monochromator. The V K-edge XAFS spectra of V_2O_3, VO_2 and V_2O_5 reference compounds were measured in transmission mode, and those of $Fe_{3-x}V_xO_4$ samples were collected in fluorescence mode with a Lytle detector and a Ti foil filter. All data analysis was performed using IFEFFIT software package. For $Fe_{3-x}V_xO_4$ samples fluorescence self-absorption corrections was carried out using Athena, which is part of IFEFFIT.

Specific surface area measurements were carried out by using the BET method on the basis of the N_2 physisorption capacity at 77 K on an ASAP 2020 instrument. All the samples were degassed at 433 K for 12 h before test.

The saturation magnetization (MS) of the series of magnetites is obtained from the Hysteresis loop, measured by a vibrating sample magnetometer MicroMag-2900 with magnetically immobilized cells.

Transmission electron microscope (TEM) observations were made with a JEOL JEM-100CXII instrument at the accelerating voltage of 100 kV. All powders were dispersed in ethanol on a carbon coated TEM copper grid.

Thermogravimetric and differential scanning calorimetry (TG–DSC) analyses were synchronously performed on a Netzsch

Table 1
Total Fe, Fe^{2+}, Fe^{3+} and V contents and chemical formula for the series of $Fe_{3-x}V_xO_4$.

Sample	C_V (%)	C_{Fe} (%)	$C_{Fe^{2+}}$ (%)	$C_{Fe^{3+}}$ (%)	Formula
Fe_3O_4	0.00	72.34	14.74	57.60	$Fe^{2+}_{0.61}Fe^{3+}_{2.39}O_4$
$Fe_{2.84}V_{0.16}O_4$	3.55	68.74	10.90	57.84	$Fe^{2+}_{0.45}Fe^{3+}_{2.39}V_{0.16}O_4$
$Fe_{2.74}V_{0.26}O_4$	5.71	66.55	17.03	49.52	$Fe^{2+}_{0.70}Fe^{3+}_{2.04}V_{0.26}O_4$
$Fe_{2.66}V_{0.34}O_4$	7.71	64.57	17.66	46.91	$Fe^{2+}_{0.73}Fe^{3+}_{1.93}V_{0.34}O_4$

STA 409 PC Instrument. About 20 mg of finely ground sample was heated in a corundum crucible from 30 to 1000 °C at a heating rate of 10 °C min^{-1} under N_2 or dry air atmosphere (60 cm^3 min^{-1} at normal temperature and pressure).

2.3. Adsorption test

Methylene blue ($C_{16}H_{18}ClN_3S_2{\cdot}3H_2O$, C.I. 52015, C.I. Basic Blue 9 trihydrate, M.W.: 373.9, certified pure) was purchased from Tianjin Kermel Chemical Reagent Company and used as received. Batch adsorption studies of MB on synthetic $Fe_{3-x}V_xO_4$ were carried out in a conical flask. The temperature was controlled at 25 °C. The initial pH of solution was adjusted by H_2SO_4 and NaOH. The suspension containing 20.0 mg dry $Fe_{3-x}V_xO_4$ and 20 mL varying concentrations of MB (20–250 mg L^{-1}) was constantly stirred for 1 h, predetermined time for achieving adsorption equilibrium. Then, the adsorbents were separated by centrifugation and the equilibrium concentration of MB was determined by UV–vis spectroscopy UV-7504 at a wavelength of 665 nm, the maximum absorption wavelength of MB. The amount (q_e) of MB retained on per gram of adsorbent at equilibrium concentration (C_e) was calculated using the equation:

$$q_e = \frac{(C_0 - C_e)V}{m} \quad (1)$$

where C_0 and C_e are the initial and equilibrium concentrations of MB in aqueous solution, V the solution volume and m is the amount of adsorbent.

2.4. Catalytic tests

The degradation experiments were carried out in a conical flask (containing 200 mL of reaction solution) at 25 °C. The dosage of catalyst was 1.0 g L^{-1} while the concentrations of MB and H_2O_2 were 0.2 and 100 mmol L^{-1}, respectively. All the experiments were carried out under constant stirring to make the catalyst well dispersed. The pH of solution (pH 10.0) was adjusted by H_2SO_4 and NaOH. Before adding H_2O_2, the suspension containing catalyst and MB was stirred for 1 h to achieve adsorption equilibrium. Then the degradation reaction was initiated by adding H_2O_2 into MB solution. At given intervals of degradation, each sample was determined by UV–vis spectroscopy UV-7504 at a wavelength of 665 nm. The magnetite after adsorption and degradation was collected and dried in a vacuum oven at 100 °C for 24 h, used for TG–DSC analysis introduced above.

3. Results and discussion

3.1. Chemical composition of magnetites

The chemical compositions of the prepared magnetites $Fe_{3-x}V_xO_4$ (Table 1) obtained from chemical analysis show that the increase of vanadium content is followed by a simultaneous decrease of the total Fe and Fe^{3+} content. This indicates that vanadium has entered into the crystal structure of magnetite and mainly replaced Fe^{3+}, which is consistent with the studies by Nivoix and Gillot [22], and Kim et al. [23]. In Fe_3O_4, the Fe^{2+} content is 14.74%, quite lower than its theoretical value (24.14%), while that of Fe^{3+} (57.60%) is higher than its theoretical value (48.28%). This suggests that some Fe^{2+} has been oxidized to Fe^{3+}. For the samples doped with vanadium, Fe^{2+} contents are also lower than their expected value, implying that Fe^{2+} in these samples has been partially oxidized. Especially for $Fe_{2.84}V_{0.16}O_4$, the extent of Fe^{2+} oxidation is the highest because its Fe^{2+} content is much less than that in the other samples, while vanadium mainly replaces Fe^{3+}.

3.2. Inverse spinel structure of magnetites

The X-ray diffraction patterns of $Fe_{3-x}V_xO_4$ are illustrated in Fig. 1. The characteristic reflections of four samples well correspond to the standard card of magnetite (JCPDS: 19-0629, not shown) [3,24]. This indicates that the synthetic magnetites have spinel structure and the incorporation of vanadium does not significantly change the crystal structure. However, the iron oxide phase of the spinel structure cannot be clearly distinguished through XRD patterns above, because of the very similar peak position, relative intensity and lattice parameters between Fe_3O_4 (magnetite) and γ-Fe_2O_3 (maghemite) [25,26]. Magnetite is an inverse spinel structure with a cubic unit cell, which consists of two sub-structure of octahedral and tetrahedral sites. The octahedral site is occupied by Fe^{2+} and half of the Fe^{3+} ions, whereas the tetrahedral site is occupied by the other half of the Fe^{3+} ions. As for maghemite, however, only Fe^{3+} ions occupy both the octahedral and tetrahedral sites. To distinguish these two phases, investigation of the existence of the Fe^{2+} is needed [27]. Therefore, in order to identify the successful synthesization of magnetite, Mössbauer measurement was carried out to provide useful information on the valence state and magnetic behavior of iron ions in a crystal lattice.

The analyses of the Mössbauer spectral parameters of the prepared magnetites (Table 2) indicate the formation of magnetite with hyperfine field (B_{hf}) of 48.98 T (tetrahedral site A) and 45.36 T (octahedral site B) with isomer shifts (ISs) 0.331 and 0.603 mm s^{-1}, respectively [28,29]. The IS value for the octahedral site is 0.603 mm s^{-1}, which is consistent with Fe^{3+} and Fe^{2+} charge states. Also, a signal with B_{hf} 50.22 T, IS 0.357 mm s^{-1} and the relative area of 10.2% suggests the presence of maghemite γ-Fe_3O_4 [30,31]. The IS value 0.357 is very consistent with Fe^{3+} charge states. For vanadium doped samples, the spectra (Fig. 2) also can be fitted with three six line patterns which are related to the octahedral and tetrahedral sites of magnetite and maghemite. The existence of maghemite results from the oxidation of magnetite, in excellent accordance with the chemical analysis.

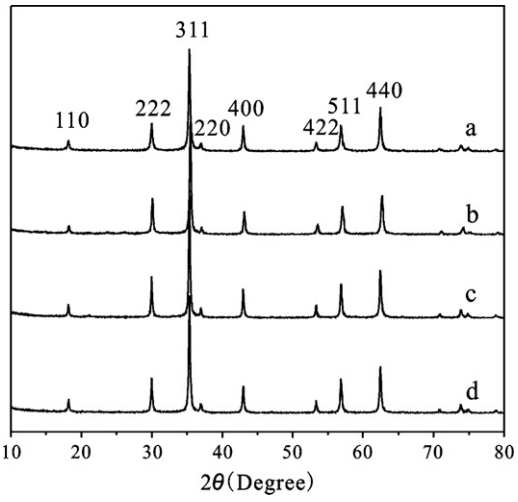

Fig. 1. X-ray diffraction patterns of the synthetic $Fe_{3-x}V_xO_4$ (a: Fe_3O_4; b: $Fe_{2.84}V_{0.16}O_4$; c: $Fe_{2.74}V_{0.26}O_4$; d: $Fe_{2.66}V_{0.34}O_4$).

Table 2
Mössbauer parameters for the $Fe_{3-x}V_xO_4$ samples.

Sample	Phase	IS (mm s^{-1}) (±0.002)	QS (mm s^{-1}) (±0.004)	B_{hf} (T) (±0.004)	Relative area (%)
Fe_3O_4	Fe_3O_4(A)	0.331	−0.004	48.696	45.9
	Fe_3O_4(B)	0.603	0.060	45.356	43.9
	γ-Fe_2O_3	0.357	0.034	50.224	10.2
$Fe_{2.84}V_{0.16}O_4$	Fe_3O_4(A)	0.325	−0.006	48.431	58.4
	Fe_3O_4(B)	0.552	0.003	44.764	23.0
	γ-Fe_2O_3	0.368	−0.010	50.142	18.6
$Fe_{2.74}V_{0.26}O_4$	Fe_3O_4(A)	0.322	0.011	48.072	39.2
	Fe_3O_4(B)	0.618	−0.002	44.919	46.3
	γ-Fe_2O_3	0.339	−0.028	48.759	14.4
$Fe_{2.66}V_{0.34}O_4$	Fe_3O_4(A)	0.342	−0.001	46.120	44.4
	Fe_3O_4(B)	0.571	−0.012	42.650	41.1
	γ-Fe_2O_3	0.323	−0.044	47.482	14.4

3.3. Valency and occupied sites of vanadium

The FTIR spectra of the prepared magnetites show two main absorption peaks in the range of 370–800 cm^{-1}, which are characteristic peaks of magnetite (Fig. 3). For Fe_3O_4, two major bands at 590 and 408 cm^{-1} are ascribed to Fe–O stretching modes of tetrahedral and octahedral sites in magnetite, respectively [32,33]. For vanadium doped magnetites, the absorption band at 408 cm^{-1} gradually shifts to higher wavenumber with the increase of vanadium content, while the band at 590 cm^{-1} remains unchanged. The shift of the band at 408 cm^{-1} should be ascribed to the change in the bonding force between the cations and the oxygen anion arising from the presence of vanadium, which presents a stronger ionic bond [34]. This indicates that vanadium mainly occupies the octahedral site.

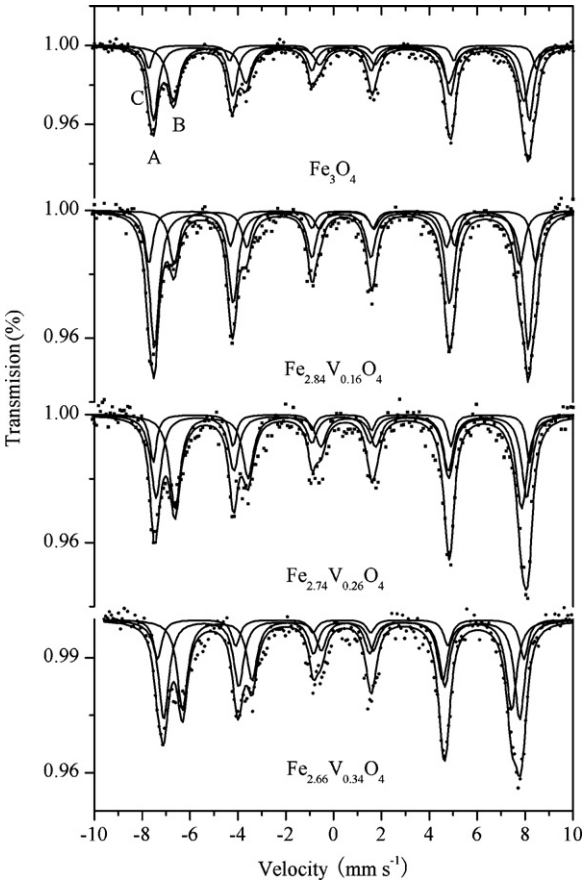

Fig. 2. Mössbauer spectra of the synthetic $Fe_{3-x}V_xO_4$ at room temperature.

FTIR is the first spectral technique used to obtain information about the valency of vanadium [35]. It has been confirmed that some absorption bands in 800–950 cm^{-1} should appear for the valency of vanadium higher than 3 [34]. The infrared spectrum of $Fe_{2.64}V_{0.36}O_4$ does not show any obvious bands in this wavenumber range (Fig. 3). However, after $Fe_{2.64}V_{0.36}O_4$ was heated at 500 °C under air for 2 h, its FTIR shows several absorption bands in the range of 800–950 cm^{-1}. The bands at ~937 and ~835 cm^{-1} are characteristic for presence of V^{5+} and V^{4+} cations, respectively. Moreover, the band at ~887 cm^{-1} is attributed to the isolated VO_4 tetrahedral where vanadium is in the valency +5 state, indicating that some of vanadium may occupy the tetrahedral site. Therefore, the appearance of these three absorption bands after oxidation shows that vanadium is in a valency state lower than +4 in initial spinel phase, similar to the real valency of vanadium in natural vanadium–titanium magnetite.

Mössbauer spectroscopy also can be used to investigate the occupied sites of doping metal through the variety of Mössbauer spectral parameters (Table 2). For $Fe_{2.84}V_{0.16}O_4$, compared with Fe_3O_4, a more pronounced decrease of the B signal occurs, like IS and B_{hf}, while little changes happen to the A signal, suggesting that vanadium prefers to occupy the octahedral site. This is consistent with the conclusions made by Junior et al. [36], and Kim et al. [23]. When the vanadium concentration increases, the parameters of B signal still obviously decrease, indicating that vanadium still preferentially occupies the octahedral site. However, with the increase of vanadium content, a substitution at the tetrahedral site seems to occur, since a small decrease appears on the parameters of A signal. This gives supporting evidence to the conclusion obtained from

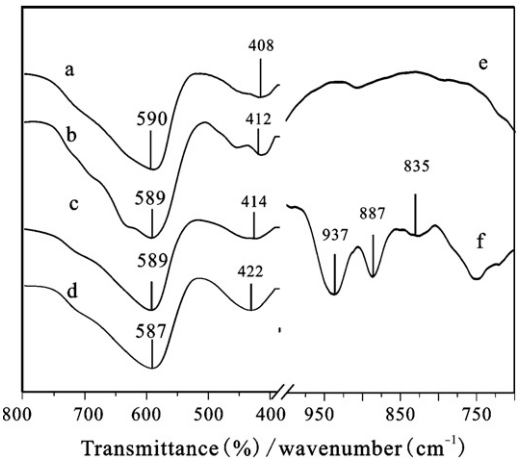

Fig. 3. FTIR spectra of the synthetic $Fe_{3-x}V_xO_4$ (a: Fe_3O_4; b: $Fe_{2.84}V_{0.16}O_4$; c: $Fe_{2.74}V_{0.26}O_4$; d and e: $Fe_{2.66}V_{0.34}O_4$; f: $Fe_{2.76}V_{0.34}O_4$ heated at 500 °C).

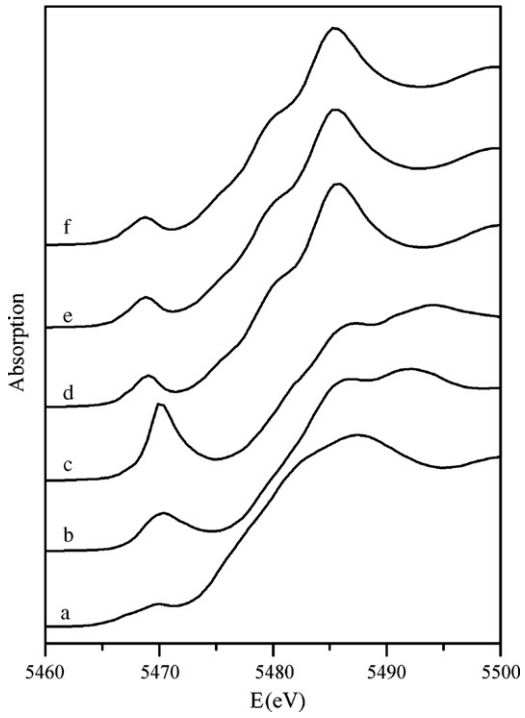

Fig. 4. XANES for series of $Fe_{3-x}V_xO_4$ and vanadium oxides (a: V_2O_3; b: VO_2; c: V_2O_5; d: $Fe_{2.84}V_{0.16}O_4$; e: $Fe_{.2.74}V_{0.26}O_4$; f: $Fe_{2.66}V_{0.34}O_4$).

FTIR that part of vanadium occupies the tetrahedral site. The phenomenon of V occupying the tetrahedral site also has been reported in other studies [36,37].

FTIR and Mössbauer spectrum mainly provide information about iron, which can indirectly show the changes of vanadium in valency and occupied site. In this study, XAFS measurement was carried out to provide direct information about vanadium. Fig. 4 shows the normalized X-ray near edge structure spectra of $Fe_{3-x}V_xO_4$ as well as V_2O_3, VO_2 and V_2O_5 as reference compounds. For V_2O_3 a very weak pre-edge peak appears at 5469.1 eV, and the absorption edge, which is defined as the maximum of derivative at the absorption edge is located at 5480.5 eV. For VO_2 a pre-edge peak is also observed at 5470.3 eV, while its intensity is much large than that of V_2O_3 and the absorption edge is located at 5483.2 eV. For V_2O_5 a very sharp pre-edge appear at 5469.9 eV and the absorption edge is at 5484.3 eV. The XANES spectrum of $Fe_{2.84}V_{0.16}O_4$ sample displays a feather rather different from those vanadium oxides. A weak pre-edge peak appears at 5468.8 eV. The absorption edge shows a strong peak with two obvious shoulders, and the energy positions are at 5474.6, 5478.6 and 5484.0 eV, respectively. While the vanadium concentration increases, the XANES spectra of $Fe_{3-x}V_xO_4$ show no distinct variation. This indicates for $Fe_{3-x}V_xO_4$, the valency state and the coordination of vanadium are almost the same.

The pre-edge peaks in the XANES spectra are attributed to the *s–d* transition. Usually the transition is dipole-forbidden, but it becomes partially allowed by mixing of the d-states of the transition metal with the p-states of the surrounding atoms. Wong et al. have studied the XANES spectra of crystallized vanadium-bearing compounds, and demonstrated that the intensity and position of the pre-edge peak depend strongly on the coordination and the valency of vanadium [38]. For $Fe_{3-x}V_xO_4$, both the intensity and energy position of the pre-edge peak is similar to that of V_2O_3. This indicates vanadium in magnetite exists as V^{3+}. Moreover, the two obvious shoulders appear clearly at the absorption edge of $Fe_{3-x}V_xO_4$. Similar structures were also observed in the XANES spectra of roscoelite ($KAlV_2Si_3O_{10}(OH)_2$), in which V^{3+} ions partially substitute Al^{3+} ions and occupy distortedly the octahedral sites. This suggests that for $Fe_{3-x}V_xO_4$, vanadium have incorporated into the lattice of magnetite and mainly occupied the octahedral site. The appearance of the pre-edge peak indicates V^{3+} ions that enter the lattice of magnetite have caused the distortion of oxygen atoms around, otherwise V^{3+} ions are in a regular octahedral symmetry and no pre-edge peak can be observed in the XANES spectra due to the relaxation of the forbidden of *s–d* transition.

3.4. Physical–chemical properties of vanadium doped magnetites

As shown in Table 3, the lattice parameter a_0 estimated from the (3 1 1) reflection in XRD patterns does not change greatly, due to its low amount of vanadium introduced and to almost the same value of cationic radii for V^{3+} (64 pm) and Fe^{3+} (65 pm) [36]. And

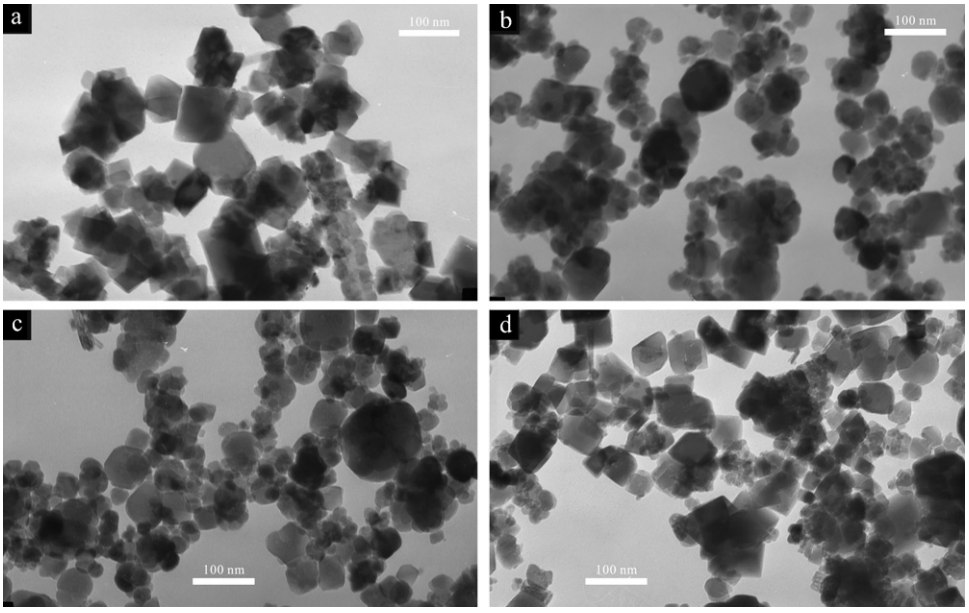

Fig. 5. TEM analyses of $Fe_{3-x}V_xO_4$ (a: Fe_3O_4; b: $Fe_{2.84}V_{0.16}O_4$; c: $Fe_{.2.74}V_{0.26}O_4$; d: $Fe_{2.66}V_{0.34}O_4$).

Table 3
Lattice parameters, particle size and BET surface area for the $Fe_{3-x}V_xO_4$.

Sample	a_0 (nm)	Particle size (nm)	Surface area ($m^2\ g^{-1}$)	Saturation magnetization ($A\ m^{-1}$)
Fe_3O_4	0.8411	28.2	27.84	69
$Fe_{2.84}V_{0.16}O_4$	0.8392	33.9	30.84	60
$Fe_{2.74}V_{0.26}O_4$	0.8408	35.0	25.90	60
$Fe_{2.66}V_{0.34}O_4$	0.8417	34.5	40.34	59

the small variety of a_0 may result from the different extent of the Fe^{2+} oxidation among these samples, because at the octahedral site the cationic radii of Fe^{2+} (78 pm) is larger than that of Fe^{3+} (65 pm) [16]. Therefore, for $Fe_{2.84}V_{0.16}O_4$, the a_0 is the least for its highest Fe^{2+} oxidation extent, which well agrees with the chemical analysis results. Table 3 also shows the average crystal size of samples calculated by the Scherrer equation. The average crystal size of samples located at 28–35 nm, suggesting that vanadium introduction does not cause an obvious change of the average crystal size. This is in accordance with the similar surface area of the four samples (25.9–40.3 $m^2\ g^{-1}$). Vanadium incorporation into the structure leads to a significant decrease in the saturation magnetization of the materials. Likewise, from Mössbauer spectroscopy, hyperfine magnetic field (B_{hf}) also decreases with the increase of vanadium content, as shown in Table 2.

Fig. 5 shows the TEM images of $Fe_{3-x}V_xO_4$. In four samples, more than 90% of the particles are in the size range of 10–100 nm. For Fe_3O_4, the presented particles show similar shape and sizes in the range of 50–70 nm. These particles are well crystallized and grow in the octahedral form. With the introduction of vanadium, the nano-particles tend to be near spherical in shape, with the average grain size obliviously decreasing. However, for sample $Fe_{2.76}V_{0.34}O_4$, most of the granules again turn to be octahedral shape and its size is mostly below 50 nm.

Thermogravimetric and differential scanning calorimetry (TG–DSC) analyses is an important technique to investigate the surface hydroxy amount and thermal stability of the material. The TG curves under N_2 (Fig. 6) show a mass loss from ca. 150 to 400 °C, corresponding to dehydroxylation and increasing with the increase of vanadium content [39]. In this study, surface hydroxyl group mainly comes from the dissociation of the water molecular adsorbed by the oxygen defect which increases with the substitution of V for Fe [40]. Therefore, the amount of surface hydroxyl group increases with the increase of V introduction.

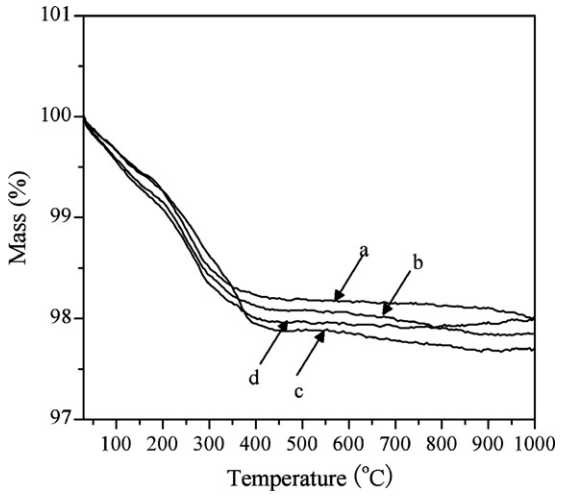

Fig. 6. The TG curves of the synthetic $Fe_{3-x}V_xO_4$ samples under N_2 (a: Fe_3O_4; b: $Fe_{2.84}V_{0.16}O_4$; c: $Fe_{2.74}V_{0.26}O_4$; d: $Fe_{2.66}V_{0.34}O_4$).

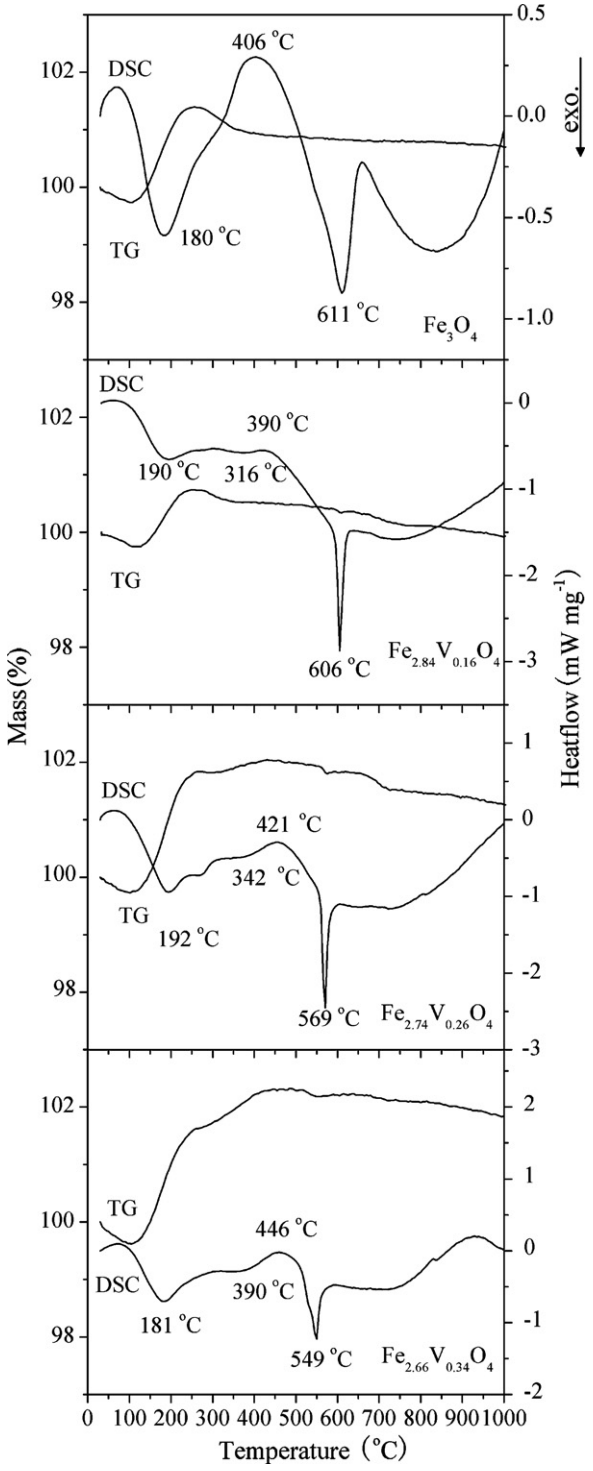

Fig. 7. The TG–DSC curves of the synthetic $Fe_{3-x}V_xO_4$ under dry air.

For Fe_3O_4 under dry air, the TG curve (Fig. 7) shows a mass gain with approximately 1.71% from ca. 150 to 300 °C, with the mass loss (0.93%) of dehydroxylation under N_2 in the same temperature range. The real mass gain from ca. 150 to 300 °C is 2.64%, related to the oxidation of Fe^{2+} to produce the phase maghemite γ-Fe_2O_3 [39,41]. The real mass gain value (2.64%) is less than the expected value to produce maghemite (3.45%), suggesting that approximately 25% of the Fe^{2+} has been oxidized to Fe^{3+}. For other samples, the mass gain in this temperature range is all less than their theoretical value. Especially for $Fe_{2.84}V_{0.16}O_4$,

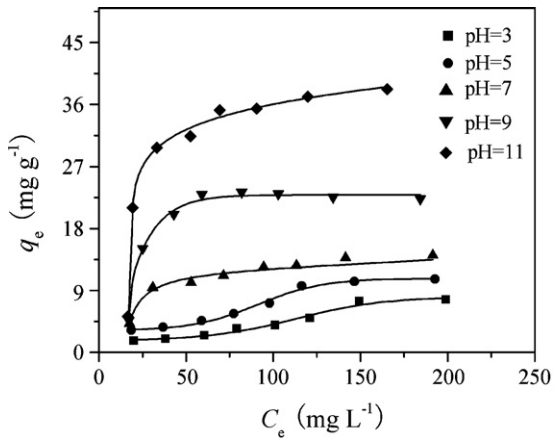

Fig. 8. Adsorption isotherms of MB onto $Fe_{2.66}V_{0.34}O_4$ at different initial pH (50 mL MB solution, 25 °C, 50 mg of $Fe_{2.66}V_{0.34}O_4$).

the mass gain in this temperature range is the least, suggesting its highest Fe^{2+} oxidation extent. DSC curves of all the four samples show two exothermic peaks in the range of 180–190 °C and 540–620 °C, ascribed to the oxidation of Fe^{2+} and phase transformation of maghemite–hematite, respectively [42]. As vanadium content increases, the phase transformation temperature from maghemite to hematite gradually decreases. Moreover, for vanadium doped magnetites, another exothermic peak appears in the range of ca. 300–400 °C, corresponding to the oxidation of vanadium [35,43]. In this temperature range, with the increase of vanadium content, the TG curves change from mass loss to mass gain, related to vanadium oxidation.

3.5. Adsorption property of $Fe_{3-x}V_xO_4$ in MB decolorization

Fig. 8 presents the influence of solution pH on the adsorption of MB onto $Fe_{2.66}V_{0.34}O_4$. It could be seen that the adsorption efficiency were strongly dependent on the initial solution pH. In the pH range of 3.0–11.0, the adsorption efficiency obviously increased with the increasing pH, indicating that the adsorption is more favorable in basic condition. The relationship between pH and absorbed amount of MB has been discussed in other studies in terms of electrostatic interactions between MB and magnetite surface [44,45]. As a cationic dye, MB ($pK_a > 12$) has a net positive charge while the pH of the solution is below 12 [46,47], which makes MB favorably adsorbed by electrostatic force onto a negatively charged adsorbent surface. In this study, the PZC of $Fe_{3-x}V_xO_4$ was about 6.96–7.05. Therefore, when the solution pH was above the pH_{ZPC}, the magnetite surface was negatively charged. The negatively charged sites on magnetite surface increased when pH increased. Hence, when the pH of MB solution increased, the complexation between MB molecules and magnetite surfaces also increased, as described in Eqs. (2) and (3):

$$Fe\text{–}OH + {}^{-}OH \leftrightarrow Fe\text{–}O^{-}H_2O \quad (2)$$

$$Fe\text{–}O^{-} + {}^{+}MB \leftrightarrow Fe\text{–}O^{-+}MB \quad (3)$$

The adsorption isotherms of MB by a series of $Fe_{3-x}V_xO_4$ at pH 7.0 (Fig. 9) show that the adsorption efficiency of $Fe_{3-x}V_xO_4$ improved with the increase of the vanadium content. The adsorption capacities (shown in Table 4) were 7.52, 10.64, 12.62 and 18.66 mg g^{-1} for Fe_3O_4, $Fe_{2.84}V_{0.16}O_4$, $Fe_{2.74}V_{0.26}O_4$ and $Fe_{2.76}V_{0.34}O_4$, respectively. In this study, the adsorption mechanism was electrostatic interactions between MB and magnetite surface. From Eq. (2), the negative charge on magnetite surface was related to the amount of surface hydroxyl above the PZC. It could be inferred that the adsorption ability was relative to the amount of surface hydroxyls.

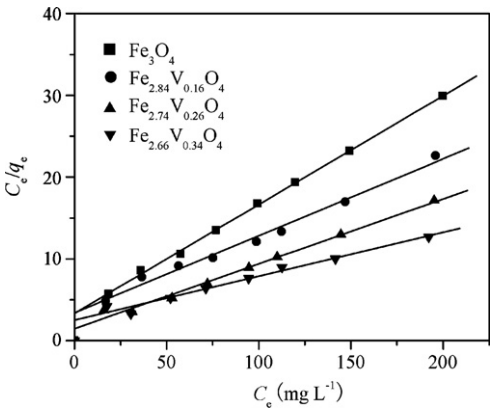

Fig. 9. Adsorption isotherms of MB onto $Fe_{3-x}V_xO_4$ at neutral pH (50 mL MB solution, pH 7.0, 25 °C, 50 mg of $Fe_{3-x}V_xO_4$).

Table 4
Langmuir isotherm constants and adsorption equations.

Sample	q_e (mg g^{-1})	q_{max}[a] (mg g^{-1})	Adsorption isotherms	R^2
Fe_3O_4	6.69	7.52	$C_e/q_e = 3.346 + 0.133C_e$	0.999
$Fe_{2.84}V_{0.16}O_4$	8.67	10.64	$C_e/q_e = 3.426 + 0.0940C_e$	0.994
$Fe_{2.74}V_{0.26}O_4$	11.42	12.62	$C_e/q_e = 1.471 + 0.0792C_e$	0.996
$Fe_{2.66}V_{0.34}O_4$	15.12	18.66	$C_e/q_e = 2.515 + 0.0536C_e$	0.989

[a] Adsorption capacity (mg g^{-1}).

From TG curves, the amount of surface hydroxyls increases with the increase of the vanadium content, which makes the improvement of adsorption activity of $Fe_{3-x}V_xO_4$. Moreover, the adsorption isotherms modelled well with the Langmuir equation.

3.6. Catalytic activity of $Fe_{3-x}V_xO_4$ in MB degradation

The catalytic activity of the series $Fe_{3-x}V_xO_4$ was investigated in decolorization of methylene blue with the presence of H_2O_2 in aqueous medium (Fig. 10). Before adding H_2O_2, the decolorization of MB only relied on the adsorption by $Fe_{3-x}V_xO_3$. The removal rate of MB by adsorption was not high in the initial condition and the highest one was about 25% for $Fe_{2.66}V_{0.34}O_4$. After the addition of H_2O_2 into the MB solution, the decolorization of MB was *via* adsorption and degradation. After 11 h, about 41, 60, 81 and 93% of MB was decolorized by Fe_3O_4, $Fe_{2.84}V_{0.16}O_4$, $Fe_{2.74}V_{0.26}O_4$ and $Fe_{2.66}V_{0.34}O_4$, respectively. The residual MB in reaction solutions decreased with the increase of V content in $Fe_{3-x}V_xO_3$. From Fig. 11,

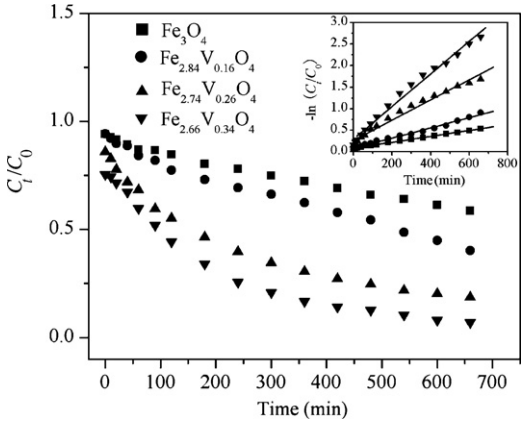

Fig. 10. Decolorization of MB by $Fe_{3-x}V_xO_4$ in the presence of H_2O_2. Inset: fitted by pseudo-first-order rate law (C_0 = 70 mg g^{-1}, 200 mL, initial pH 10.0, 25 °C, 200 mg of $Fe_{3-x}V_xO_4$).

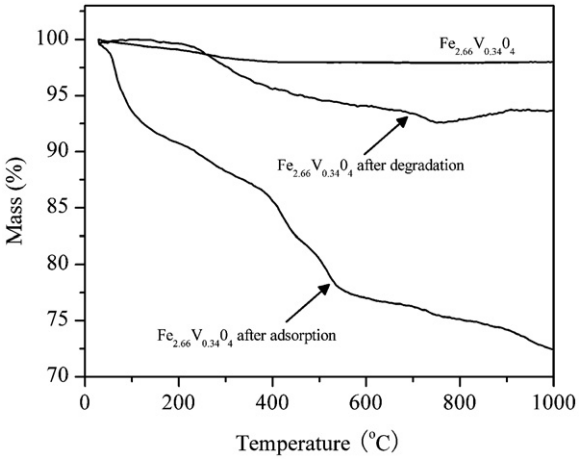

Fig. 11. TG curves under N_2 for $Fe_{2.66}V_{0.34}O_4$, $Fe_{2.66}V_{0.34}O_4$ after adsorption and $Fe_{2.66}V_{0.34}O_4$ after degradation.

it can be seen that amount of the organic matter adsorbed on the magnetite after degradation was much less than that after adsorption. Therefore, after degradation the amount of MB absorbed on catalyst were quite low. The decolorization of MB mainly resulted from the degradation catalyzed by $Fe_{3-x}V_xO_3$.

The changes of pH in each reaction system were quite obvious. The initial pH in the systems is 10.0. After the addition of H_2O_2, the pH rapidly dropped in the first 1 h, due to the appearance of several medium acidic products [48,49]. After 12 h, the pH value was about 7.7, 7.3, 6.8 and 6.7 for the systems presented with Fe_3O_4, $Fe_{2.84}V_{0.16}O_4$, $Fe_{2.74}V_{0.26}O_4$ and $Fe_{2.66}V_{0.34}O_4$, respectively. The change of pH was more oblivious when the catalyst contained more vanadium. From former research [50], when the pH of the solution is above 4.0, the amount of dissolved iron ion is so low that the effect of homogeneous Fenton reaction on the degradation process can be neglected. In this study, pH during the degradation process kept above 6.0, thus it can be observed that the whole decomposition of MB was heterogeneous Fenton reaction.

3.7. The effect of vanadium on the catalytic activity of magnetite

In this study, the removal of MB after the addition of H_2O_2 is attributed to the degradation of MB on $Fe_{3-x}V_xO_4$. Previous studies indicated that the degradation of MB followed an •OH-mediated radical mechanism [11,19]. Once a •OH radical is generated on the surface of $Fe_{3-x}V_xO_4$, it will decompose MB adsorbed on magnetite. Therefore, the degradation rate of MB is proportional to the adsorbed amount of MB and the concentration of •OH radical. Obviously, high adsorption capacity for MB is benefit for the degradation rate of the dye. However, the relationship between degradation rate and adsorbed amount of the dye should not be a linear relationship, because the degradation rate is also influenced by the concentration of •OH radical.

It has been established that the octahedral sites are almost exclusively exposed at the surface of the spinel crystallites and that the catalytic activity is mainly due to octahedral cations. In this study, iron and vanadium on the octahedral site can activate H_2O_2 in the following two reactions [51–53]:

$$\equiv Fe_{surf}{}^{3+} + H_2O_2 \rightarrow \equiv Fe_{surf}{}^{2+} + {}^{\bullet}OOH + H^+ \quad (4)$$

$$\equiv Fe_{surf}{}^{2+} + H_2O_2 \rightarrow \equiv Fe_{surf}{}^{3+} + {}^{\bullet}OH + H^+ \quad (5)$$

The incorporation of Cr, Mn and Co favors the oxidation of methylene dye. One point of their role in the reaction is that these cations on the magnetite surface can produce radicals according to the reaction:

$$\equiv M_{surf}{}^{n+} + H_2O_2 \rightarrow \equiv M_{surf}{}^{(n+1)+} + {}^{\bullet}OH + OH^- \quad (6)$$

where $M_{surf}{}^{n+}$ donates the cations Cr^{3+}, Mn^{2+} and Co^{2+} on the magnetite surface [11].

In this study, the activation of vanadium towards H_2O_2 is believed to follow the two steps below:

$$\equiv V_{surf}{}^{3+} + H_2O_2 \rightarrow \equiv Fe_{surf}{}^{4+} + {}^{\bullet}OH + H^+ \quad (7)$$

$$\equiv V_{surf}{}^{4+} + H_2O_2 \rightarrow \equiv Fe_{surf}{}^{3+} + {}^{\bullet}OOH + H^+ \quad (8)$$

Both the metal ions on magnetite surface could activate H_2O_2 to produce active free radicals •OH. Moreover, an electron transfer during the reaction also has been used to explain the strong effect of transition metal substitution on the catalytic activity of magnetite. In this study, based on the standard reduction potentials for the metals:

$$Fe^{3+} + 1e^- \rightarrow Fe^{2+}, \qquad E^0 = 0.77\,V \quad (9)$$

$$VO^{2+} + 2H^+ + 1e^- \rightarrow V^{3+} + H_2O, \qquad E^0 = 0.361\,V \quad (10)$$

$$Fe^{3+} + V^{3+} \rightarrow Fe^{2+} + V^{4+}, \qquad E^0 = 0.409\,V \quad (11)$$

From Eq. (11), it can be seen that the reduction of Fe^{3+} by V^{3+} is thermodynamically favorable, producing Fe^{2+}, greatly active for the initial step of Fenton reaction.

On the other hand, the reduction potential V^{3+} to V^{2+} is similar to the potential involved in the redox pair Fe^{2+}/Fe^{3+}:

$$V^{3+} + 1e^- \rightarrow V^{2+}, \qquad E^0 = -0.255\,V \quad (12)$$

Based on this redox potential, the reduction of Fe^{3+} by V^{2+} is in favor of the regeneration of Fe^{2+} in the Fenton reaction. Eq. (13) suggests that this process is also thermodynamically favorable. The V^{2+} species could be reproduced by the reduction with H_2O_2 or •OOH.

$$Fe^{3+} + V^{2+} \rightarrow Fe^{2+} + V^{3+}, \qquad E^0 = 1.025\,V \quad (13)$$

From the above equations, the effect of vanadium introduction on the catalytic activity is also due to improving the electron transfer during the reaction and efficiently regenerating the active specie Fe^{2+}.

4. Conclusions

In conclusion, the present study has determined the valency and occupied sites of vanadium, the physical–chemical properties, adsorption and catalytic activities of the doped magnetite, making it possible to connect its structure with activity during the MB decolorization. The characterization results show that the synthetic vanadium doped magnetites have inverse spinel structure, with part of Fe^{2+} oxidized to Fe^{3+}. Vanadium in magnetite is in valency +3 and preferentially occupies the octahedral sites. The vanadium substitution leads to the increase of superficial hydroxyls, a decrease of temperature of phase transformation maghemite–hematite and magnetism. The substitution of vanadium improves the adsorption of MB on magnetite, related to the increase of superficial hydroxyl. Meanwhile, vanadium incorporation promotes the catalytic activity of magnetite in degradation of MB *via* a heterogeneous Fenton mechanism. Vanadium on the magnetite surface can activate H_2O_2 to produce •OH. The vanadium incorporation also promotes the electron transfer during the reaction and produces a more efficient regeneration of the Fenton active specie Fe^{2+}. The obtained new insights are of high importance for well understanding the transference and transformation of organic contaminants on the earth surface, the design of novel catalysts and the utilization of natural magnetite in the field of environmental science.

Acknowledgements

This is contribution No. IS-1176 from GIGCAS. We would like to thank Beijing Synchrotron Radiation Facility for giving us the beam time for the XAFS measurement. This work is supported by National Natural Science Foundation of China (Grant No. 40773060) and "863" Exploration Program, the Ministry of Science and Technology of the People's Republic of China (Grant No. 2006AA03Z337).

References

[1] F.Q. Gan, J.M. Zhou, H.Y. Wang, C.W. Du, X.Q. Chen, Water Res. 43 (2009) 2907–2915.
[2] X.C. Wei, R.C. Viadero, Colloid Surf. A 294 (2007) 280–286.
[3] A.J. Tchinda, E. Ngameni, I.T. Kenfack, A. Walcarius, Chem. Mater. 21 (2009) 4111–4121.
[4] N. Mukaihata, H. Matsui, T. Kawahara, H. Fukui, H. Tada, J. Phys. Chem. C 112 (2008) 8702–8707.
[5] L. Zampori, P.G. Stampino, G. Dotelli, Appl. Clay Sci. 42 (2009) 605–610.
[6] R. Sennour, G. Mimane, A. Benghalem, S. Taleb, Appl. Clay Sci. 43 (2009) 503–506.
[7] Q. Zhou, H.P. He, J.X. Zhu, W. Shen, R.L. Frost, P. Yuan, J. Hazard. Mater. 154 (2008) 1025–1032.
[8] K.H. Chung, K.Y. Lee, J. Hazard. Mater. 172 (2009) 922–927.
[9] A.H. Lu, S.J. Zhong, J. Chen, J.X. Shi, J.L. Tang, X.Y. Lu, Environ. Sci. Technol. 40 (2006) 3064–3069.
[10] M. Hermanek, R. Zboril, N. Medrik, J. Pechousek, C. Gregor, J. Am. Chem. Soc. 129 (2007) 10929–10936.
[11] R.C.C. Costa, M.F.F. Lelis, L.C.A. Oliveira, J.D. Fabris, J.D. Ardisson, R.R.V.A. Rios, C.N. Silva, R.M. Lago, J. Hazard. Mater. 129 (2006) 171–178.
[12] V.S. Coker, C.I. Pearce, R.A.D. Pattrick, G. Van der Laan, N.D. Telling, J.M. Charnock, E. Arenholz, J.R. Lloyd, Am. Mineral. 93 (2008) 1119–1132.
[13] P.S. Sidhu, R.J. Gilkes, A.M. Posner, J. Inorg. Nucl. Chem. 40 (1978) 429–435.
[14] A. Khan, P. Chen, P. Boolchand, P.G. Smirniotis, J. Catal. 253 (2008) 91–104.
[15] M.A. Ahmed, N. Okasha, M.M. El-Sayed, Ceram. Int. 33 (2007) 49–58.
[16] F. Magalhaes, M.C. Pereira, S.E.C. Botrel, J.D. Fabris, W.A. Macedo, R. Mendonca, R.M. Lago, L.C.A. Oliveira, Appl. Catal. A-Gen. 332 (2007) 115–123.
[17] M.F. Zhou, P.T. Robinson, C.M. Lesher, R.R. Keays, C.J. Zhang, J. Malpas, J. Petrol. 46 (2005) 2253–2280.
[18] M.F. Zhou, C.Y. Wang, K.N. Pang, G.J. Shellnutt, Y. Ma, Mineral Deposit Research: Meeting the Global Challenge, Vols. 1 and 2, Springer Berlin Heidelberg, 2005, pp. 511–513.
[19] S.J. Yang, H.P. He, D.Q. Wu, D. Chen, X.L. Liang, Z.H. Qin, M.D. Fan, J.X. Zhu, P. Yuan, Appl. Catal. B: Environ. 89 (2009) 527–535.
[20] W. Yu, T.L. Zhang, H. Zhang, X.J. Qiao, L. Yang, Y.H. Liu, Mater. Lett. 60 (2006) 2998–3001.
[21] J.W. Di, Y.F. Tu, Y. Wu, D.Q. Liu, Spectrosc. Spect. Anal. 22 (2002) 800–802.
[22] V. Nivoix, B. Gillot, Solid State Ionics 111 (1998) 17–25.
[23] K.J. Kim, S.L. Choi, Y.R. Park, J.H. Lee, J.Y. Park, S.J. Kim, J. Magn. Magn. Mater. 310 (2007) E876–E877.
[24] H.P. Qi, J. Ye, N. Tao, M.H. Wen, Q.W. Chen, J. Cryst. Growth 311 (2009) 394–398.
[25] C.M. Wang, D.R. Baer, J.E. Amonette, M.H. Engelhard, J. Antony, Y. Qiang, J. Am. Chem. Soc. 131 (2009) 8824–8832.
[26] D.C. Cook, S.J. Oh, R. Balasubramanian, M. Yamashita, Hyperfine Interact. 122 (1999) 59–70.
[27] H.M. Lee, Y.R. Uhm, C.K. Rhee, J. Alloy Compd. 461 (2008) 604–607.
[28] K. Woo, J. Hong, S. Choi, H.W. Lee, J.P. Ahn, C.S. Kim, S.W. Lee, Chem. Mater. 16 (2004) 2814–2818.
[29] A. Bandhu, S. Mukherjee, S. Acharya, S. Modak, S.K. Brahma, D. Das, P.K. Chakrabarti, Solid State Commun. 149 (2009) 1790–1794.
[30] F.C.C. Moura, M.H. Araujo, R.C.C. Costa, J.D. Fabris, J.D. Ardisson, W.A.A. Macedo, R.M. Lago, Chemosphere 60 (2005) 1118–1123.
[31] M.I. Shukoor, F. Natalio, M.N. Tahir, M. Divekar, N. Metz, H.A. Therese, P. Theato, V. Ksenofontov, H.C. Schroder, W.E.G. Muller, W. Tremel, J. Magn. Magn. Mater. 320 (2008) 2339–2344.
[32] M. Mandal, S. Kundu, S.K. Ghosh, S. Panigrahi, T.K. Sau, S.M. Yusuf, T. Pal, J. Colloid Interface Sci. 286 (2005) 187–194.
[33] G. Gnanaprakash, J. Philip, T. Jayakumar, B. Raj, J. Phys. Chem. B 111 (2007) 7978–7986.
[34] M. Nohair, D. Aymes, P. Perriat, B. Gillot, Vib. Spectrosc. 9 (1995) 181–190.
[35] V. Nivoix, B. Gillot, Mater. Chem. Phys. 63 (2000) 24–29.
[36] I.L. Junior, J.M.M. Millet, M. Aouine, M. do Carmo Rangel, Appl. Catal. A-Gen. 283 (2005) 91–98.
[37] J.Y. Park, J.H. Lee, K.J. Kim, J. Korean Phys. Soc. 53 (2008) 695–699.
[38] J. Wong, F.W. Lytle, R.P. Messmer, D.H. Maylotte, Phys. Rev. B 30 (1984) 5596–5610.
[39] D. Thickett, M. Odlyha, J. Therm. Anal. Calorim. 80 (2005) 565–571.
[40] F. Finocchi, J. Goniakowski, Phys. Rev. B 6412 (2001).
[41] J.P. Sanders, P.K. Gallagher, J. Therm. Anal. Calorim. 72 (2003) 777–789.
[42] E. Kester, B. Gillot, P. Perriat, P. Dufour, C. Villette, P. Tailhades, A. Rousset, J. Solid State Chem. 126 (1996) 7–14.
[43] B. Gillot, V. Nivoix, Mater. Res. Bull. 34 (1999) 1735–1747.
[44] R.C. Wu, J.H. Qu, Water Environ. Res. 76 (2004) 2637–2642.
[45] M.A. Al-Ghouti, M.A.M. Khraisheh, M.N.M. Ahmad, S. Allen, J. Hazard. Mater. 165 (2009) 589–598.
[46] C.A.P. Almeida, N.A. Debacher, A.J. Downs, L. Cottet, C.A.D. Mello, J. Colloid Interface Sci. 332 (2009) 46–53.
[47] R.G. Harris, J.D. Wells, B.B. Johnson, Colloid Surf. A 180 (2001) 131–140.
[48] H. Ma, Q. Zhuo, B. Wang, Environ. Sci. Technol. 41 (2007) 7491–7496.
[49] A. Houas, H. Lachheb, M. Ksibi, E. Elaloui, C. Guillard, J.M. Herrmann, Appl. Catal. B: Environ. 31 (2001) 145–157.
[50] S.S. Chou, C.P. Huang, Y.H. Huang, Environ. Sci. Technol. 35 (2001) 1247–1251.
[51] S.S. Lin, M.D. Gurol, Environ. Sci. Technol. 32 (1998) 1417–1423.
[52] W.P. Kwan, B.M. Voelker, Environ. Sci. Technol. 37 (2003) 1150–1158.
[53] J.H. Deng, J.Y. Jiang, Y.Y. Zhang, X.P. Lin, C.M. Du, Y. Xiong, Appl. Catal. B: Environ. 84 (2008) 468–473.